SAND2020-8236C

Solution Mining Research Institute Fall 2020 Virtual Technical Conference

22-24 SEPTEMBER 2020

PIPE PERFORATION VS STRING CUTS FOR LEACHING MITIGATION

David B. Hart [1], Gavin P. Fleming [2], John R. Torczynski [1], Dean A. Checkai [2], and Martin B. Nemer [1]

[1] Sandia National Laboratories, Albuquerque, NM, USA

[2] Fluor Federal Petroleum Operations, New Orleans, LA, USA

Abstract

The U.S. Strategic Petroleum Reserve (SPR) is in the process of selling oil based on mandates from the U.S. Congress. SPR's configuration makes it necessary to remove oil from storage caverns using fresh to saline water instead of brine. As a result, oil sales change cavern shapes due to dissolution of the salt. The impact on shape depends on the volume of raw water, the original cavern shape, the depth to the brine string end of tubing, and the location of the oil-brine interface. The effects that some well configurations have had on the cavern shape, particularly near the cavern floor, will be presented.

Two methods have been identified in order to move the effective injection point and mitigate effects on cavern floor shape: string cuts and string perforation. String cuts reduce string length but impact the ability to run logs through the string. Effects due to string cuts are relatively straightforward to model and predict. On the other hand, string perforation adds another pathway for brine movement but depends heavily on fluid mechanics. Most perforation work described in the literature has dealt with fluid flowing into open air, rather than into a dense fluid such as brine. Other oil/gas-related research has focused on flow into a perforated pipe from oil reservoirs, which is a very different problem. Here, the fluid mechanics for water flowing down a vertical perforated pipe into brine were examined.

The model indicates that, for appropriate flow regimes, raw water would exit the perforations and not the end of tubing. A field scale test to validate the model was designed and implemented using cavern BM-102 during recent oil sales. Sonar surveys were taken before and after the oil removal to gather cavern geometry data for comparison. The results of the field test and the model validation analysis are presented.

Key words: Caverns for Liquid Storage, Fluid Mechanics, Computer Modeling, Cavern Dissolution Experiments, Cavern Hydraulics, Pipe Perforation, DOE, Strategic Petroleum Reserves

Sandia National Laboratories is a multimission laboratory managed and operated by National Technology and Engineering Solutions of Sandia, LLC, a wholly owned subsidiary of Honeywell International, Inc., for the U.S. Department of Energy's National Nuclear Security Administration under contract DE-NA0003525. Fluor Federal Petroleum Operations (FFPO) is a special-purpose company formed for the sole purpose of managing and operating the Strategic Petroleum Reserve (SPR) under a prime contract with the U.S. Department of Energy (DOE). This paper describes objective technical results and analysis. Any subjective views or opinions that might be expressed in the paper do not necessarily represent the views of the U.S. Department of Energy or the United States Government.

Nomenclature

10 ¾"	shorthand in this document for a standard SPR brine string, including all specifications
3D	three-dimensional
API	American Petroleum Institute (standards organization)
BC	boundary condition
BHF	Braden head flange
BM	Bryan Mound
BS	brine string
DOE	U.S. Department of Energy
EOT	end of tubing
FFPO	Fluor Federal Petroleum Operations
GEM	Gun Evaluation Model
ID	inner diameter
ISO	International Standards Organization
MD	measured depth
OBI	oil-brine interface
OD	outer diameter
ODE	ordinary differential equation
perf	perforation
SNL	Sandia National Laboratories
SPR	U.S. Strategic Petroleum Reserve

Units – US customary and petroleum industry specific

"	inches (used here only when identifying API casing or tool sizes)
bbl	oil barrel (≡ 42 US gallons ≈ 158.987 L)
cP	centipoise (≡ 0.001 Pa s)
ft	foot (≡ 0.3048 m)
in	inch (≡ 0.0254 m)
lbf	pound-force (≈ 4.44822 N)
Mbbl	thousand barrels
MBH	thousand barrels per hour
MMbbl	million barrels
psi	pound-force per square inch (≈ 6894.76 Pa)
psig	psi, gauge (i.e., relative to atmospheric conditions)

WH	West Hackberry

Introduction

The U.S. Strategic Petroleum Reserve (SPR) is comprised of 60 underground storage caverns used for storing liquid crude oil. The caverns are located at four sites in Louisiana and Texas, along the Gulf Coast. The SPR has a maximum authorized capacity of 727 MMbbl (115.584 × 10^6 m^3). The U.S. Congress passed several laws requiring oil to be sold from the SPR, on the open market, in order to help fund various initiatives.

Due to the initial design and mission of the SPR, which involved static storage in preparation against a continuous drawdown over 90 days to meet an emergency need, releases from the SPR were designed to use raw water – undersaturated brine with a maximum salinity of sea water. Using undersaturated brine causes leaching to occur during a release from the SPR, however during a full emergency drawdown, this leaching would occur in an onion-skin-like layer around the entire cavern surface. The caverns were designed to be able to handle at least five of such emergency drawdowns.

Previous events, such as Hurricane Katrina, have resulted in the need for relatively small releases, or partial drawdowns, from the SPR; e.g., on the order of millions of barrels (hundreds of thousands of cubic meters) of oil spread across multiple caverns and sites. These are usually referred to as exchanges, where oil is released from the SPR and then oil is returned months to a year later once the emergency has passed. This also results in the oil/brine interface (OBI) moving up and then down repeatedly over the same, relatively small region of the cavern, resulting in localized leaching.

Of particular concern, significant widening in the foot over a relatively narrow depth area has been observed; in this paper, such shapes will be referred to as “flippers” (see Figure 1 for illustrations). While geomechanical analysis has not shown any serious concern with feet that have developed at any SPR caverns so far, prudence dictates that mitigation measures should be considered prior to any problems occurring.

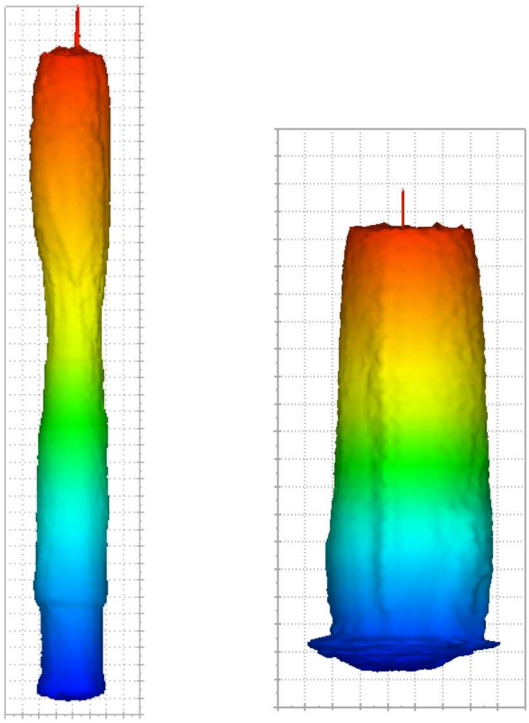

Figure 1 Left: example of ledges created at the end of tubing (EOT) when the EOT is significantly above the floor, but still close to the OBI. Right: example of “flippers” where significant expansion occurs in a narrow range at the base of the cavern. Grid squares are 50 ft (15.24 m) to a side.

Both modeling and field observations have shown that the greatest leaching effect occurs at the depth of the end of the hanging string (end-of-tubing, EOT) and tapers upward to the OBI. One obvious method of mitigating localized leaching is move the EOT further up above the cavern floor. This would require a rig intervention, which is feasibly unattractive, or cutting the brine string (BS). The standard method used historically was to sever the BS at the desired depth using an explosive jet cutter or split shot wireline tool and allow the cut brine string to fall to the bottom of the cavern.

An alternative option to severing the pipe would be to perforate the brine string at predetermined depths up-hole, nearer to the OBI or other preferred depths prior to the mandatory oil sales. (Mitigation is less feasible in the case of emergency events, which only increases the importance of mitigation when partial drawdowns are pre-planned, like during sales). This alternative method was thought to have multiple advantages in addition to helping re-distribute the leaching effect to a shallower depth and move the circulation point from the EOT to the perforated interval in the BS. Benefits also include:

- avoiding potentially problematic material from collecting on the cavern floor,
- allowing recovery of undamaged pipe from below the perforations during future rig workovers,
- and reducing the likelihood of damage to logging tools run down the string due to ragged cuts.

This paper describes the testing of this mitigation approach, from preliminary modelling up to a field-scale, operational beta test. A mathematical model for calculating the perforations necessary to move all flow to the perforations was developed, and tools developed for use in the field tests. The gun (perforation tool) configuration was evaluated in both surface/bench tests and in a separate down-hole test where the hanging string was recovered for analysis. Finally, the field-scale operational test was conducted in an SPR cavern during the Fall 2019 sales cycle, with pre- and post-fluid movement sonar surveys conducted to evaluate the performance of the perforated string.

Perforated Pipe Flow Mathematical Model

A model for the flow of raw water through a hanging string having a section with perforations is developed that includes buoyancy forces in the raw water inside the tube and the saturated brine outside the tube. These forces lead to a critical inlet velocity below which all of the raw water flows out the perforations and none of the raw water flows out the end of tube. Previous research found in the literature has focused on the flow from a pipe into the atmosphere (Bailey, 1975) or on the flow from a formation into a pipe (see Clemo, 2006), however, no studies focused on the vertical pipe flow of one liquid into a different liquid, as would occur in SPR caverns.

Figure 2 shows diagrams of an SPR cavern and the brine string (BS), including the EOT at the lower end. When injecting raw water through the hanging string, some fraction of the raw water exits the perforations laterally into the cavern, and the remainder of the raw water exits the EOT near the bottom of the cavern.

Figure 2 also shows diagrams of the five flow states that are expected based on unequal buoyancy forces. These states are delineated below. In States 1-4, all raw water flows out the perforations, and no raw water flows out the EOT. In State 5, some raw water flows out the perforations, and some raw water flows out the EOT.

1. When the inlet velocity is very slow, a raw water/brine interface exists in the perforated region.
2. At a certain fairly slow inlet velocity, this interface reaches the bottom of the perforated region.
3. At slightly higher inlet velocities, this interface is between the perforated region and the EOT.
4. At a somewhat higher “critical” inlet velocity, the raw water/brine interface reaches the EOT.
5. When the inlet velocity exceeds this critical value, no raw water/brine interface exists in the tube.

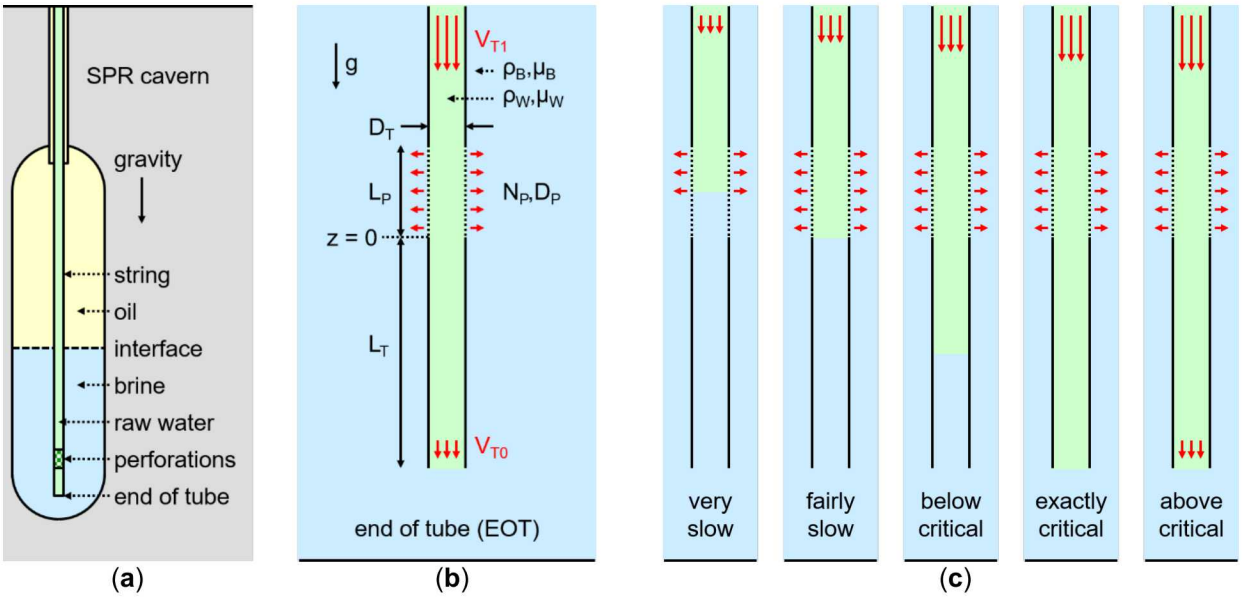

Figure 2 (**a**) Diagram of SPR cavern.
(**b**) Diagram of end of tube and perforations with variables.
(**c**) Flow states in region between perforations and EOT with inlet velocities increasing from left to right. The dimensions and relative velocities are not to scale.

The model of Nemer and Kassam (2019) and Torczynski (2019) is presented below and is based on an earlier model of Bailey (1975), who investigated a similar situation but on a vastly smaller scale than SPR. Their revised model includes unequal buoyancy forces in the raw water and the brine. If buoyancy is neglected, the ratio of the outlet velocity to the inlet velocity is constant. If buoyancy is included, this ratio decreases as the inlet velocity is decreased, and a critical inlet velocity exists below which the outlet velocity is zero.

Two simplifications are made from the full differential equation model developed by Nemer and Kassam from the Bailey model. First, instead of considering very many discrete perforations, the perforations are represented as a uniform distribution of perforation area per unit length of tube. This converts very many difference equations into a few ordinary differential equations (ODEs) and boundary conditions (BCs). Second, the Darcy-Weisbach friction factor f_D and the discharge coefficient C_d are taken to be their limits for infinite Reynolds number (reasonable for an SPR application). This model yields the critical inlet velocity below which the outlet velocity at the EOT is zero and the outlet velocity as a function of the inlet velocity when the inlet velocity is above this critical value.

The model assumes that raw water fills the tube and thus applies for States 4-5, as in Figure 2:

$$0 \le z \le L_p: \qquad \frac{dp_h}{dz} = (\rho_B - \rho_W)g, \qquad \frac{dp_T}{dz} = \frac{f_D}{D_T}\frac{\rho_W}{2}V_T^2, \qquad \frac{dV_T}{dz} = \frac{A_P C_d}{L_P A_T}\sqrt{\frac{2(p_H + p_T)}{\rho_W}}; \qquad \text{(ODEs)}$$

$$z = 0: \qquad p_H[0] = (\rho_B - \rho_W)gL_T, \qquad p_T[0] = p_{T0} = \frac{f_D L_T}{D_T}\frac{\rho_W}{2}V_{T0}^2, \qquad V_T[0] = V_{T0}; \qquad \text{(BCs)}$$

$$f_D \to \frac{1}{\left(2\log\frac{3.7D_T}{k_T}\right)^2}, \qquad C_d \to 0.63. \qquad \text{(infinite Reynolds number)}$$

Here, ρ_B and ρ_W are the brine and raw-water densities, g is the gravitational acceleration, p_H is the hydrostatic (or buoyant) pressure difference (i.e., inside minus outside), p_T is the friction-factor pressure, V_T is the raw-water mean velocity over the tube cross section, p_{T0} and V_{T0} are the values of these

quantities at $z = 0$ (i.e., the bottom of the perforated section), z is the vertical coordinate, D_T is the tube diameter, D_P is the diameter of a single perforation, L_T and L_P are the lengths of the sections of tube without and with perforations, $A_T = \pi D_T^2/4$ is the tube cross-sectional area, $A_P = N_P \pi D_P^2/4$ is the total cross-sectional area of the perforations, N_P is the number of perforations, C_d is the discharge coefficient, f_D is the Darcy-Weisbach friction factor, and k_T is the roughness height on the tube inner surface.

Recognizing that $p_T \ll p_H$ and evaluating the ODE source terms at $z = L_P/2$ (the midpoint of the perforated section) yields a closed-form approximation for the inlet velocity, $V_{T1} = V_T[L_P]$, which additionally can be evaluated for $g = 0$ (zero gravity, so zero buoyancy) to quantify the effect of buoyancy:

$$V_{T1,\mathrm{appr}} = \frac{A_P C_d}{A_T}\sqrt{\frac{2(p_{HM} + p_{TM})}{\rho_W}} + V_{T0}, \quad p_{HM} = (\rho_B - \rho_W) g L_M, \quad p_{TM} = \frac{f_D L_M}{D_T}\frac{\rho_W}{2} V_{T0}^2; \quad (\mathrm{approx.,buoyancy})$$

$$V_{T1,\mathrm{nogr,appr}} = \left(1 + \frac{A_P C_d}{A_T}\sqrt{\frac{f_D L_M}{D_T}}\, V_{T0}\right); \quad L_M = L_T + \frac{L_P}{2} \qquad (\mathrm{approx.,no\ buoyancy})$$

Setting the outlet velocity to zero yields the critical inlet velocity: $V_{T1,\mathrm{crit}} = V_T[L_P]$ with $V_{T0} = 0$. It is noted that the ODE/BC system is most easily solved parametrically by specifying V_{T0} and finding V_{T1}.

These equations are evaluated using *Mathematica* (Wolfram, 2019). The function NDSolve with its default settings is used to solve the ODE/BC system numerically. Table 1 provides example parameter values for a test case.

Table 1 Parameters and values that are reasonable but may not represent any particular situation.

Quantity	Symbol	Example Value(s)
Brine density	ρ_B	sg = 1.2 (1200 kg/m^3)
Raw-water density	ρ_W	sg = 1.0 (1000 kg/m^3)
Oil density	ρ_O	sg = 0.9 (900 kg/m^3)
Brine viscosity	μ_B	1 cP (0.001 Pa s)
Raw-water viscosity	μ_W	1 cP (0.001 Pa s)
Oil viscosity	μ_O	5 cP (0.005 Pa s)
Oil-brine surface tension	σ_{OB}	0.0148 lbf/ft (0.02 N/m)
Gravitational acceleration	g	32 ft/s^2 (9.8 m/s^2)
Inlet velocity of raw water	V_{T1}	0-30 ft/s (0-9.1 m/s)
Length of cavern	L_C	2000 ft (609.6 m)
Diameter of cavern	D_C	200 ft (60.96 m)
Length of tube without perforations	L_T	50 ft (15.24 m)
Length of tube with perforations	L_P	20 ft (6.096 m)
Inner diameter of tube	D_T	9.85 in (25.0 cm)
Inner diameter of a perforation	D_P	0.4–0.7 in (1–1.8 cm)
Mean wall roughness height of tube	k_T	0.04 in (1 mm)
Number of perforations	N_P	200
Discharge coefficient of a perforation	C_d	0.63, could be 0.5–1.0
Darcy-Weisbach friction factor for tube	f_D	$1/(2\log(3.7D_T/k_T))^2$
Cross-sectional area of tube	A_T	$\pi D_T^2/4$
Total cross-sectional area of perforations	A_P	$N_P \pi D_P^2/4$

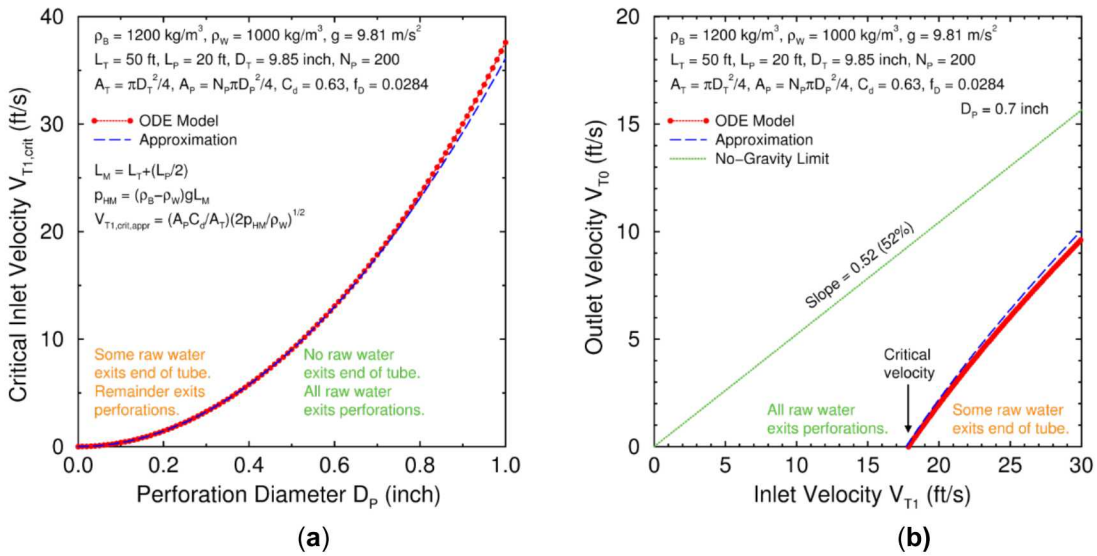

Figure 3 Left: Critical inlet velocity versus perforation diameter for indicated conditions. Right: Outlet velocity versus inlet velocity for indicated conditions. (1 ft = 0.3048 m, 1 inch = 0.0254 m.).

Figure 3 shows the critical inlet velocity $V_{T1,\mathrm{crit}}$ versus the perforation diameter D_P. The approximation for $V_{T1,\mathrm{crit}}$ depends quadratically on D_P since $A_P = N_P \pi D_P^2/4$. Values from the ODE/BC model and the approximation agree closely. For perforation diameters of D_P = 0.4–0.7 in (1.0–1.8 cm), the critical inlet velocities are $V_{T1,\mathrm{crit}}$ = 6–18 ft/s (1.8–5.5 m/s), which significantly overlaps the typical range of interest: V_{T1} = 10–30 ft/s (3.0–9.1 m/s).

Figure 3 also shows the outlet velocity V_{T0} (below the perforated section) versus the inlet velocity V_{T1} (above the perforated section) for a perforation diameter of D_T = 0.7 in (1.8 cm). Below the critical inlet velocity of $V_{T1,\mathrm{crit}}$ = 18 ft/s (5.5 m/s), no raw water flows out the EOT: $V_{T0} = 0$. Above the critical inlet velocity, the outlet velocity V_{T0} increases almost linearly with the inlet velocity V_{T1}, in accord with the approximation and the fact that $p_{TM} \ll p_{HM}$. However, as the inlet velocity becomes large, the outlet velocity V_{T0} bends over and approaches the no-gravity limit, which, for this case, has a slope of 0.52 so that the outlet velocity is 52% of the inlet velocity. These limiting values are in accord with those of Nemer and Kassam (2019).

The model results depend weakly on the Darcy-Weisbach friction factor f_D (which in turn depends weakly on the wall roughness height k_T) but depend strongly on the discharge coefficient C_d of the perforations. This quantity depends strongly on the perforation shape and can vary from 1 to below 0.5 (Batchelor, 1967). Thus, the model results can have order-unity uncertainty based on this quantity.

This model could be incorporated into *SANSMIC* (Russo, 1983; Weber et al., 2016) to quantify the effect of injecting raw water through perforations on cavern shape.

Perforation feasibility testing

The feasibility of using perforations to adjust BS injection depth was originally considered with respect to hydraulics; injection pressure is required to inject raw water down the BS to the EOT and allow the raw water to displace and move the oil out of the cavern during sales. As water has a higher specific gravity than oil, the water will stay below the OBI. However, two important considerations with this approach were: (1) to ensure that the total flow area created by the perforations would not restrict flow during oil sales, and (2) not cause a split or partial injection between the perforations and the EOT.

Two work objectives were identified to physically and mathematically verify that preferential flow could be obtained through the use of perforations. The first step was to ensure that the total flow area of all the perforations would be equal to or greater than the flow area of the BS: a 10 ¾" outer diameter (OD) 51 pound per foot (ppf) (27.3 cm, 73.75 kg/m^3), J-55 grade, 8rd ST&C casing. (This is the standard SPR BS, and for brevity will be referred to simply as «the 10 ¾"»). The 10 ¾" BS has an internal diameter $D_T =$ 9.85 in (25.0 cm).

The BS has a total flow area $A_T = 76.16$ in^2 (491.4 cm^2). Investigation work to identify what type of perforating gun system would be required to obtain this minimum flow area, and determine a method to verify the results, was developed. Tools developed from the mathematical model to support this calculation were used to design the perforation target: $N_P = 200$ perforations with a diameter $D_P = 0.7$ in (1.78 cm).

Perforation tool selection

Perforating Services are available from the existing wireline service contractor for the SPR. Preliminary work with our contractor and their sub-contractor for perforating charges, was initiated to determine the feasibility of perforating the brine string to develop the minimum required flow area. Use of their perforating performance software allowed for review and selection of gun system and perforating charges made available under the contract.

The standard gun systems available under contract were limited to sizes below 5 in (12.7 cm) diameter gun carriers. However, the sub-contractor had a large range of available perforating charge selection in order to establish the minimum flow area from perforations. As establishing the minimum flow area with the perforations was considered critical for success, verification testing was developed and planned. The test objectives were to execute, collect, and evaluate the condition of the casing joint, validation of the performance of the perforating guns, system, and actual effects to the bring string. The WH-109 well was scheduled for a diagnostic workover and was selected as a good candidate for this test.

Gun size and charge type were reviewed and selected using pre-test model runs made with the Gun Evaluation Model (GEM) to simulate downhole perforating conditions. Selection criteria was prioritized based on maximum flow area per gun run. Model runs depicting casing weight, grades, formation type, fluid type, orientation and gun types were made and compared for gun and charge size selection. Available gun type per existing contract allowed for selection of Titan 4 5/8" (11.8 cm), 22.7 gram-weight HMX BH gun system with shot phasing of 135/45° and loading at 12 shots per foot (approximately 39 shots per meter).

Feasibility Test in Cavern WH-109

The perforating gun test execution was completed on May 20, 2019 in the West Hackberry Cavern Well 109 as per procedure by perforating from 4336 to 4354 ft (1321.6–1327 m) measured depth below the Braden head flange (BHF) on the wellhead; all depths in this report will be in measured depth referenced to the BHF. The perforated joint of the 10 ¾" BS was later pulled and laid out for inspection on May 23, 2019. Visual inspection with photos was conducted to evaluate the condition of the pipe, indication of deformation, gauged ID and OD, number of shots, entry hole sizes, perforation conditions, and burr sizes. The casing joint has been retained should further work or information be needed to complete test. The collected data is documented and referenced.

The overall condition of the perforated casing appeared normal with no splitting or severe damage (see Figure 4). Some swelling occurred near the exit holes of the perforations with the largest increase in outer diameter drift measurement of 0.2 in (5 mm). External perforating burrs were also seen with protruded measurements from base of pipe 0.25 to 0.35 in (6.35–8.89 mm).

Figure 4 shows that the perforated entry hole sizes varied considerably for the eight planes or orientation positions of the gun charges. The gun was detonated in the de-centralized position with indication that the low side of the gun laid between two orientation positions of the gun charges. Entry hole sizes varied widely from the largest entry hole, $D_P = 0.90$ in (22.86 mm), to the smallest entry hole, $D_P = 0.175$ in (4.45 mm). Due to the decentralized positioning of the guns, the smaller entry holes were located on the high side position of the gun. Figure 5 presents the hole diameters for each of the arms of the gun.

Figure 4 Perforated casing with entry hole diameter variance due to gun decentralization. From top of photo wrapping towards the bottom, this shows holes from rows 6, 3, 8, and 5 (see Figure 5).

With each entry hole measured from the test, a comparison was made of actual perforated surface flow area to the GEM model's prediction. The test showed that 51% of the modeled surface area was realized due to reduced entry hole sizes in the actual results. Further investigation of the model identified that the predicted performance diminishes when the water gap, the space between the explosive and the pipe, is greater than 3 in (7.62 cm). During the test, some positions were at a maximum water gap of 5.35 in (13.6 cm) due to the guns being decentralized. However, based on these test results, it was determined that the total perforation entry hole size and area needed to be increased by 2 times to the desired flow area. It was further recommended that an additional 20% increase of the total area be used until further testing can confirm consistent perforating performance.

Based on the results from the perforating test in WH-109 the final recommendation from FFPO was made to proceed with a beta test during the 2019 fall oil sales, and SNL recommended using cavern BM-102 from the among the caverns that would be used in the sales. The beta test would use this modified perforating method to effectively shorten the brine string in well BM-102B; due to the uneven perforations seen in the feasibility test, the total number of perforation entry holes would need to be increased by 140% to achieve the minimum desired flow area.

	Row 1	Row 2 *	Row 3	Row 4 *	Row 5 *	Row 6	Row 7 *	Row 8
	0°	225°	90°	315°	180°	45°	270°	135°
				Hole Diameter (inches)				
1	0.51	0.182	0.9	0.243	0.214	0.86	0.175	0.48
2	0.53	0.182	0.87	0.243	0.214	0.82	0.175	0.51
3	0.5	0.182	0.86	0.243	0.214	0.83	0.175	0.61
4	0.53	0.182	0.83	0.243	0.214	0.82	0.175	0.53
5	0.46	0.182	0.81	0.243	0.214	0.84	0.175	0.49
6	0.58	0.182	0.86	0.243	0.214	0.85	0.175	0.47
7	0.48	0.182	0.83	0.243	0.214	0.84	0.175	0.4
8	0.51	0.182	0.74	0.243	0.214	0.83	0.175	0.42
9	0.55	0.182	0.83	0.243	0.214	0.81	0.175	0.4
10	0.46	0.182	0.8	0.243	0.214	0.78	0.175	0.41
11	0.55	0.182	0.82	0.243	0.214	0.75	0.175	0.38
12	0.4	0.182	0.75	0.243	0.214	0.82	0.175	0.38
13	0.48	0.182	0.72	0.243	0.214	0.76	0.175	0.35
14	0.44	0.182	0.8	0.243	0.214	0.82	0.175	0.39
15	0.51	0.182	0.78	0.243	0.214	0.87	0.175	0.4
16	0.59	0.182	0.75	0.243	0.214	0.86	0.175	0.34
17	0.47	0.182	0.79	0.243	0.214	0.82	0.175	0.38
18	0.44	0.182	0.8	0.243	0.214	0.73	0.175	0.33
19	0.43	0.182	0.76	0.243	0.214	0.81	0.175	0.37
20	0.49	0.182	0.73	0.243	0.214	0.72	0.175	0.35
21	0.49	0.182	0.63	0.243	0.214	0.8	0.175	0.37
22	0.34	0.182	0.71	0.243	0.214	0.67	0.175	0.37
23	0.51	0.182	0.74	0.243	0.214	0.8	0.175	0.33
24	0.4	0.182	0.67	0.243	0.214	0.82	0.175	0.35
25	0.41	0.182	0.67	0.243	0.214	0.81	0.175	**Missing ****

Figure 5 Entry hole diameter measurements from the 10 ¾" casing specimen. Each gun arm rotates 135° per layer. Asterix indicates that row is significantly below average size with restricted flow. (*SI units omitted for clarity, multiply values by 25.4 to convert to millimeters*).

Field Scale Beta Test in Cavern BM-102

Selection of the cavern to use for the beta test involved evaluation of various criteria for suitability. The current cavern geometry, current OBI depth, oil volume, and the age of the brine string were all considered. Of particular importance was to ensure that:

- the leaching would occur where sonar surveys would be able to differentiate between a successful and unsuccessful mitigation result, i.e., the cavern was not overly wide,
- there were no existing features that would be adversely affected by an unsuccessful test, and
- there was sufficient distance between the starting OBI, the EOT, and desired perforation location that it would be observable whether the leaching occurred at the EOT or at the perforations.

Cavern Bryan Mound 102 fit the cavern criteria and well BM-102B was in an acceptable brine string configuration, and so BM-102B was selected for the beta test. Cavern BM-102 was originally mined in the 1980's and is configured as a two-well cavern – BM-102C is a 13 3/8" OD (33.97 cm) slick well and BM-102B has a 10 ¾" hanging brine string of the same type described previously. The cavern had a total volume at of 11.14 MMbbl (1.771×10^6 m^3) at the time of the August 2019 sonar survey and contained 9.997 MMbbl (1.589×10^6 m^3) of crude oil. The OBI was located at 3958 ft MD (1206 m MD) and the end

of the brine string was located at a depth of 4232 ft MD (1290 m MD). The cavern is approximately 2020 ft (616 m) tall. Cavern diameters range from 150 ft (46 m) to 300 ft (91 m).

Figure 6 shows the shape of the cavern in the sonar surveys from 2003, 2013, and 2019 (the pre-experiment sonar). The changes that have occurred in the cavern over the 16 years shown can be seen: some cavern creep in the top half of the cavern, some floor rise, and some changes in the shape of the foot of the cavern due to its previous usage in partial drawdowns. The pre-sales sonar was taken on August 14, 2019, and the post-sales sonar, which will be shown later, was taken March 17, 2020.

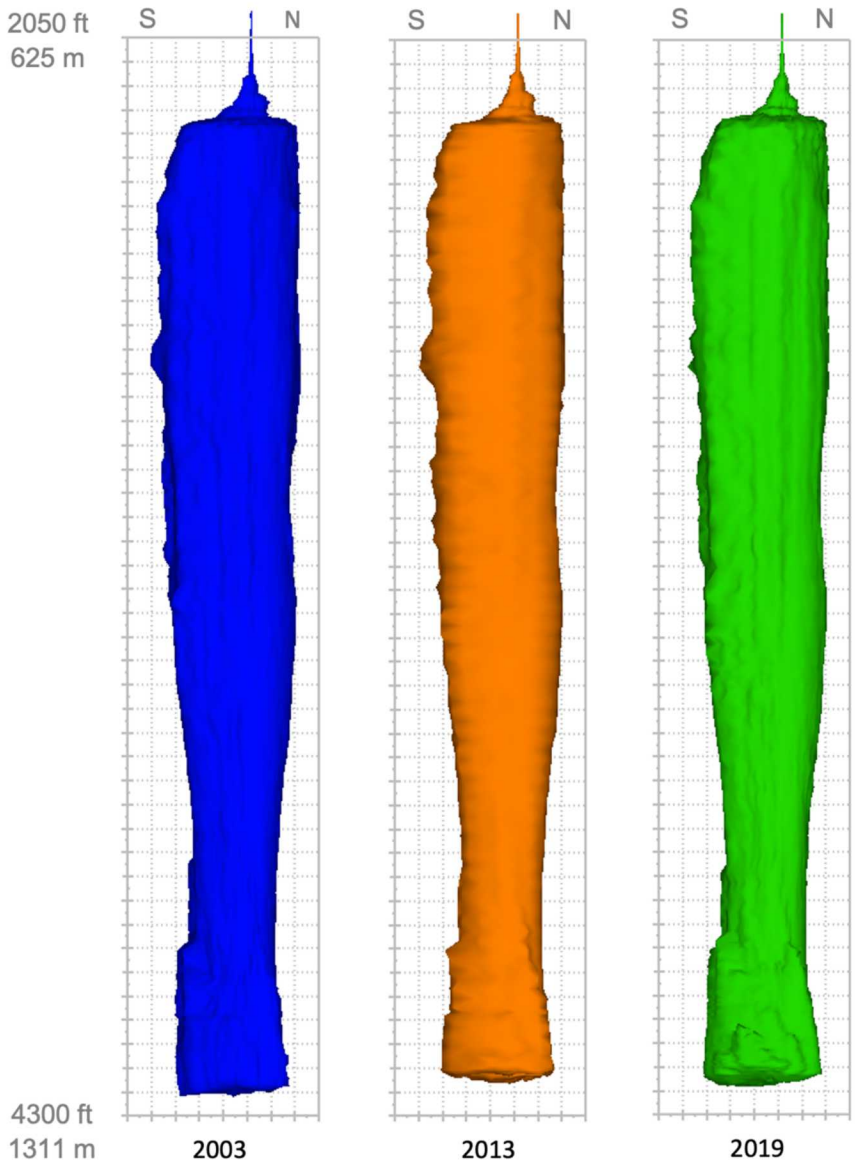

Figure 6 Cavern sonar survey history for Cavern BM-102. Grid squares are 50 ft (15.24 m) in each direction. Cavern shape is a view from the east looking west.

Perforation configuration

Based on the perforating gun performance test results from the brine string in well WH-109, it was determined that a total of 700 perforations would be required to create enough entry holes to provide the minimum required perforation flow area. The 10 ¾" brine string was perforated on September 27, 2019, using the same 4 ½" x 20 ft perforating gun used at WH-109, loaded at 12 shots per foot (39 shots per meter). Three runs were made to add a total of $N_P = 720$ holes over the interval 4023 to 4062 ft MD (1226–1238 m MD). This gave a perforated interval $L_P = 39$ ft (11.88 m) and a length of tubing below the perforations of $L_T = 170$ ft (51.8 m).

The percent of total volume that would go through the perforations was modeled and confirmed from the newly built mathematical perforation flow model. The parameters for the test are given in Table 2. Setting $V_{T0} = 0$, the calculated value of $V_{\text{crit}} = 37.7$ ft/s (11.5 m/s), which is above the maximum string velocity used at the SPR; converted, this yields a maximum flow rate of 12.77 Mbbl/h (2030 m^3/h) to avoid flow exiting from the EOT.

Table 2 Parameters for the perforation flow model based on the field beta test configuration.

Quantity	**Symbol**	**Value**	
Brine density	ρ_B	sg = 1.20	(1200 kg/m^3)
Raw-water density	ρ_W	sg = 1.01	(1010 kg/m^3)
Discharge coefficient of a perforation	C_d	0.63	
Mean wall roughness height of tube	k_T	0.01 in	(0.254 mm)
Darcy-Weisbach friction factor for tube	f_D	0.038100046	
Length of tube with perforations	L_P	39 ft	(11.88 m)
Length of tube below perforations	L_T	170 ft	(51.8 m)
Inner diameter of tube	D_T	9.85 in	(25.0 cm)
Inner diameter of a perforation (*average*)	D_P	0.41 in	(1.04 cm)
Number of perforations	N_P	720	
Cross-sectional area of tube	A_T	76.2 in^2	(491 cm^2)
Total cross-sectional area of perforations	A_P	95.3 in^2	(613 cm^2)
Target flow out EOT	V_{T0}	0 ft/s	(0 m/s)
Critical velocity (*max. to avoid flow out EOT*)	$V_{\text{crit,appx}}$	37.7 ft/s	(11.5 m/s)
Critical flow rate (*max. to avoid flow out EOT*)	$F_{\text{crit,appx}}$	12.77 Mbbl/h	(2030 m^3/h)
Minimum velocity to use all perfs.	$V_{\text{semi,crit}}$	12.0 ft/s	(3.69 m/s)
Minimum flow rate to use all perfs.	$F_{\text{semi,crit}}$	4.09 Mbbl/h	(650 m^3/h)

The minimum velocity and flow rate indicated in Table 2 are calculated using a value of $L_T = 0$; i.e., providing the minimum flow needed to push the brine/water interface just past the deepest perforation. This is in contrast to the critical flow values which calculated the flow needed to push the brine/water interface to the very bottom of the brine string. There is no downside to using flow regimes in the very slow velocity range except that flow will be distributed across only a portion of the perforated section. Figure 7 shows how different flow velocities impact the location of the oil/water interface within the brine string.

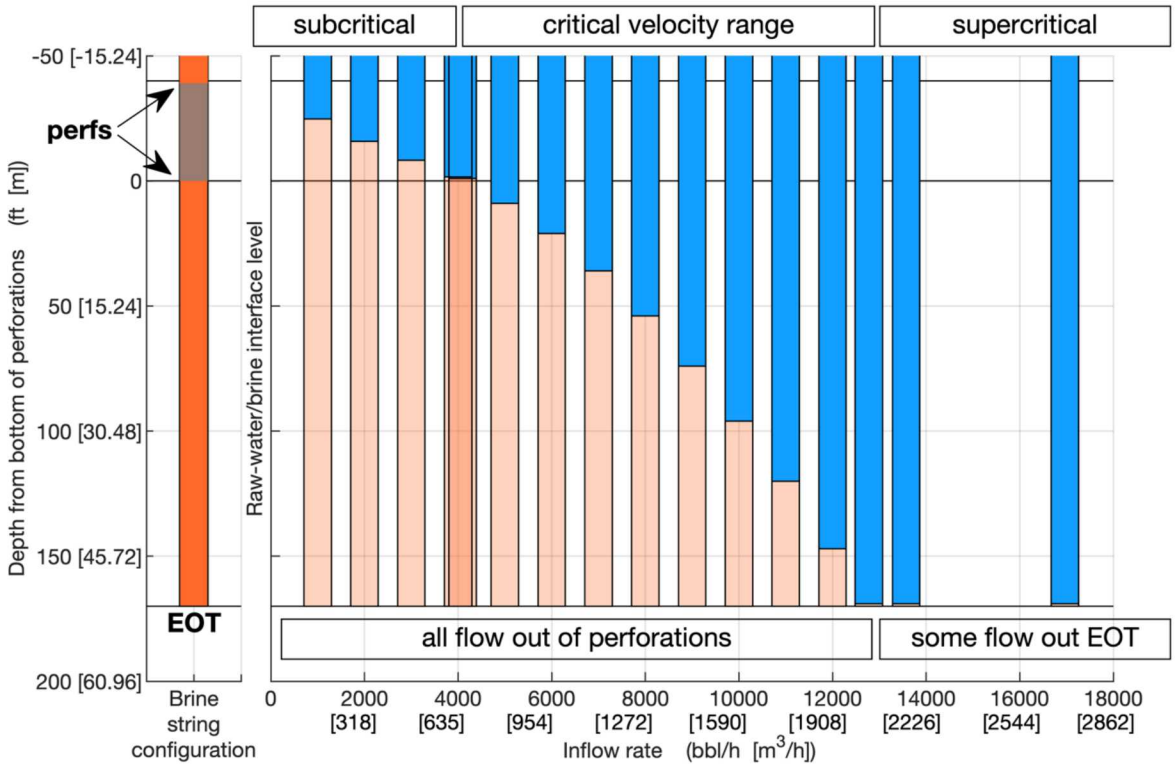

Figure 7 Left – brine string configuration showing perforated section (x-scale exaggerated). Right – location of raw-water/brine interface within the brine string at various inflow rates.

Fluid movements

Oil sales were conducted in October and November of 2019. A total of 295,492 bbl (47.0 × 10^6 m^3) of raw water was injected, in three batches, removing 276,760 bbl (44.0 × 10^6 m^3) of oil from the cavern. Flow rates were typically held between 4000 to 5000 bbl/h (636–795 m^3/h). The volume of each batch, and the corresponding flow rates, are shown in Figure 8. Comparing the flow rates to the ranges shown in Figure 7 and the critical velocities in Table 2, it is clear that all flow is expected to have exited the pipe through the perforations.

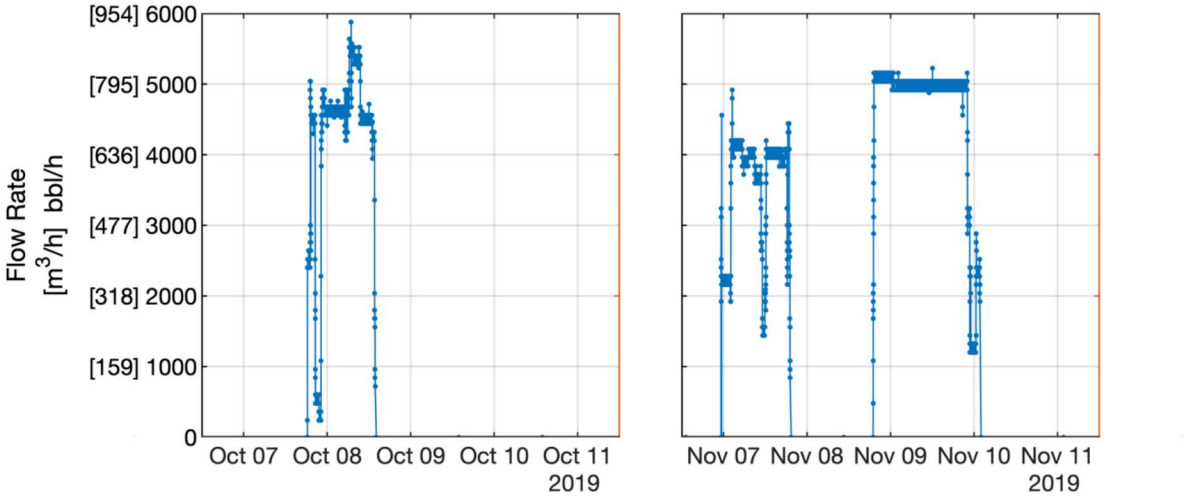

Figure 8 Raw water flow rates for each of the three sales batches that occurred in BM-102 in 2019.

During the crude oil sales period, displacement performance was monitored and compared. Injection and displacement discharge pressures and rates were monitored with no abnormal or unexpected variations in rates or pressures. For comparison purposes, Cavern BM-110 was also monitored for pressure during sales (to obtain the flow volumes needed, either three or four caverns are used simultaneously to withdraw oil). Figure 9 shows a graphical comparison of the injection pressure minus discharge pressure versus time for the two caverns.

Injection, displacement discharge pressures and rates were monitored with no abnormal or unexpected variations in rates or pressures. Interpretation from the comparison indicates that the perforated interval in the BS did not cause excess back pressure on the injection pumps and success was achieved in allowing sufficient fluid flow during oil sales. As can be seen in Figure 9, the back pressure on the pumps was less in BM-102 – the string with the perforations – as the injection depth was shallower, and thus the pressure required to overcome the hydrostatic gradient was reduced.

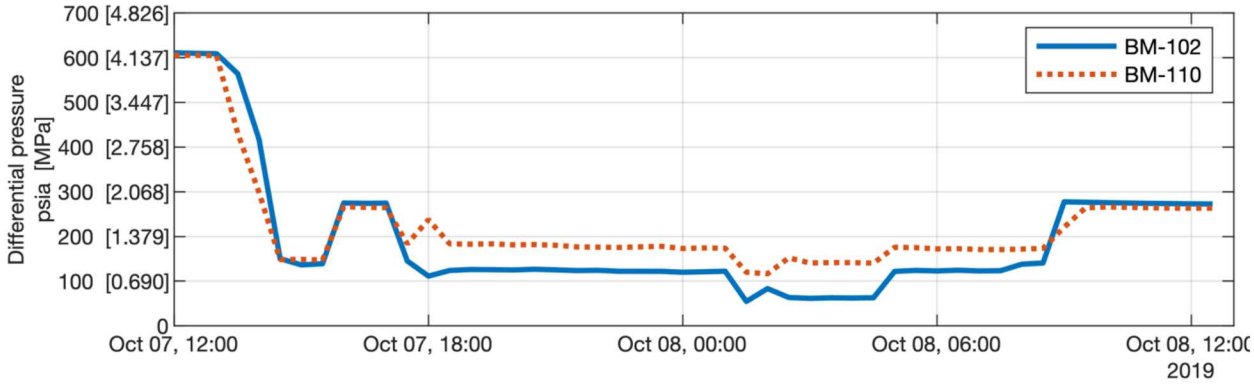

Figure 9 Delta pressure vs. time during October 7-8, 2019 oil sales, comparing caverns BM-102 and BM-110.

The cavern was held static for 30 days between the end of the first oil sales batch and the start of the second and third batches, and for approximately 129 days between the final raw water injection and the final sonar survey, where leaching occurred. Raw water has a maximum theoretical leaching efficiency of 16 to 17% based on temperature, so it was expected that the total cavern size should increase by 47 to 50 Mbbl (7500-7900 m^3) due to leaching.

Sonar Analysis

The follow up sonar survey was conducted on March 17, 2020. During the survey analysis, the representative echo was selected according to the level of amplitude, transmission time, density of measured points, and shape of the cavern. Figure 10 shows a graphical comparison of the pre- and post-sales surveys. The figure provides a 3D rendered image of the cavern surface, as viewed from the south. Additionally, several cross sections are provided at depths of particular interest.

The comparison of the sonar survey parameters is provided in the Table 3. Note that the sonar survey accuracy is presumed to be one percent of the total volume, meaning the total change in volume, both observed and expected, is less than the margin of error when looking at the entire cavern.

Table 3 Comparison of sonar surveys for BM-102, pre- and post-sales cycle.

Description	Units	August 2019	March 2020	Notes
Speed of sound (SOS) in oil medium	ft/s *m/s*	[4223, 4295] *[1287, 1309]*	4302 *1311*	SOS difference is a result of different oil composition
Speed of sound (SOS) in brine medium	ft/s *m/s*	5933.7 *1808.6*	5935.7 *1809.2*	
Datum used for depth		Braden head flange (BHF)	Braden head flange (BHF)	
Depth of 16'' casing shoe reference	ft *m*	1988 *605.9*	1988 *605.9*	
Depth of oil-brine interface	ft *m*	3958 *1206.4*	3859 / 3867 *1176.2 / 1178.7*	In 2020, sludge layer created: oil-sludge IF / sludge-brine IF
Wellhead oil pressure	psi *MPa*	695 *4.78*	684 *4.72*	
Number of runs		2	2	
Well used for survey		C-well	C-well	
Number of horizontal sections		144	152	More horizontal sections taken in 2020 survey
Number of total tilted sections		67	72	More tilted shots taken in 2020 survey
Upward tilted sections		41	52	
Downward titled sections		26	20	
Highest point of cavern	ft *m*	1988 *605.9*	1988 *605.9*	
Lowest point of cavern	ft *m*	4246.6 *1294.4*	4251.3 *1296.8*	Depth change may be due to different tiled shot locations
Total cavern volume	bbl m^3	11,142,255 *1,771,477*	11,236,857 *1,786,517*	Total volume change: 0.84% +94,602 bbl (*+15,041* m^3)

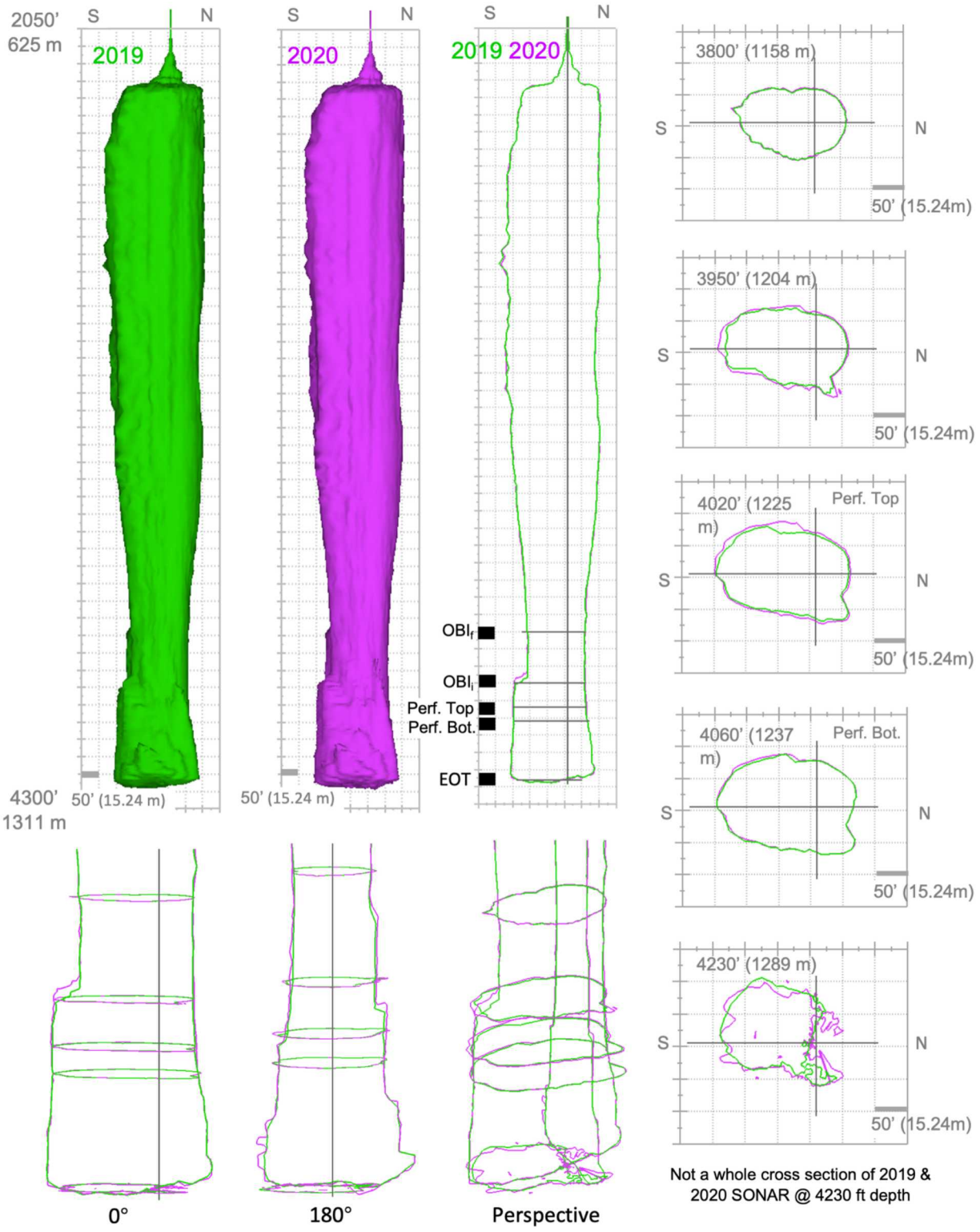

Figure 10 Comparison between the 2019 and 2020 sonar surveys; 3d renderings and cross sections are provided and depths of primary interest (perforations, OBIs, and EOT).

Among the features that are particularly intriguing is the large change just above the initial OBI at 3950 ft (1158 m) depth. It is easy to attribute this seemingly new feature to a salt fall or preferential leaching – and these hypotheses cannot be discounted – however, the original oil-brine interface would have blocked any tilted shots from within the brine from "seeing" the feature. Once the OBI was moved, two tilted stations were able to "see" this feature in the returns. Thus, the possibility of this feature being, at the least somewhat larger than originally suspected in 2019, must be considered along with the other causes.

Of additional interest is the feature that is first seen in Figure 10 in the cross section through the depth of the top of the perforations (4020 ft, 1225 m). It appears that there is a preferentially leached section just south of west at this depth. In Figure 11, radial slices are shown which include the feature. The radial sections show a feature that corresponds roughly to the depth of the perforations where more of the wall has been leached away compared to the average impact (e.g., like the areas between the two OBIs).

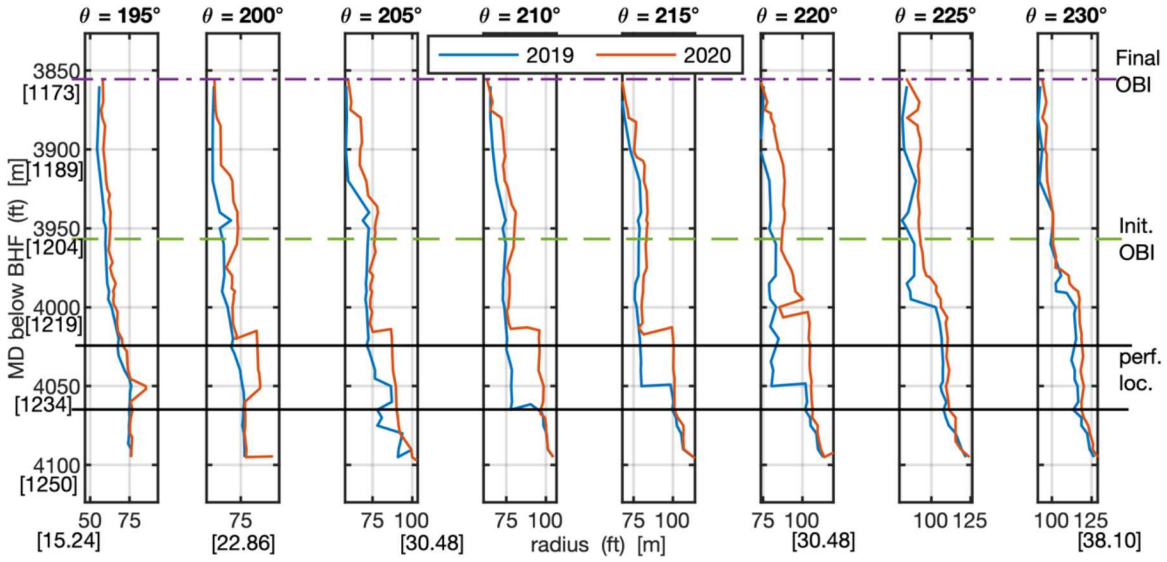

Figure 11 Radial profiles (radius vs. depth) for eight different cross sections. Angle θ represents degrees anticlockwise from East (180° = W, 225° = SW).

There are multiple reasons that this seemingly preferential leaching may have occurred at the same depth as the perforations. One possibility is that the largest hole diameters were on the same side as this feature, and therefore this is an effect of having fresh water jetted at the wall. However, it is not possible to determine the orientation of the perforation holes within the brine string at this time. Another possibility is that a salt fall occurred. There is no evidence of a large fall on the cavern floor, however. Finally, it is possible that, due to the Bryan Mound salt dome's more heterogeneous salt composition, and higher impurity ratio compared to other SPR sites, that this section simply leached more than other sections of the wall.

Another aspect of the surveys that quickly becomes clear is that, while the cross sections do show changes in radius at the depth of the original OBI and at the top of perforations, 3D and cross section analyses are difficult to evaluate with respect to the leaching effects. Along with the limitations on total cavern volume, it makes sense to look at the volume profile versus depth and focus analysis only on the bottom portion of the cavern. Figure 12 provides the volume profile for both the full cavern and for only the part of the cavern below the final OBI.

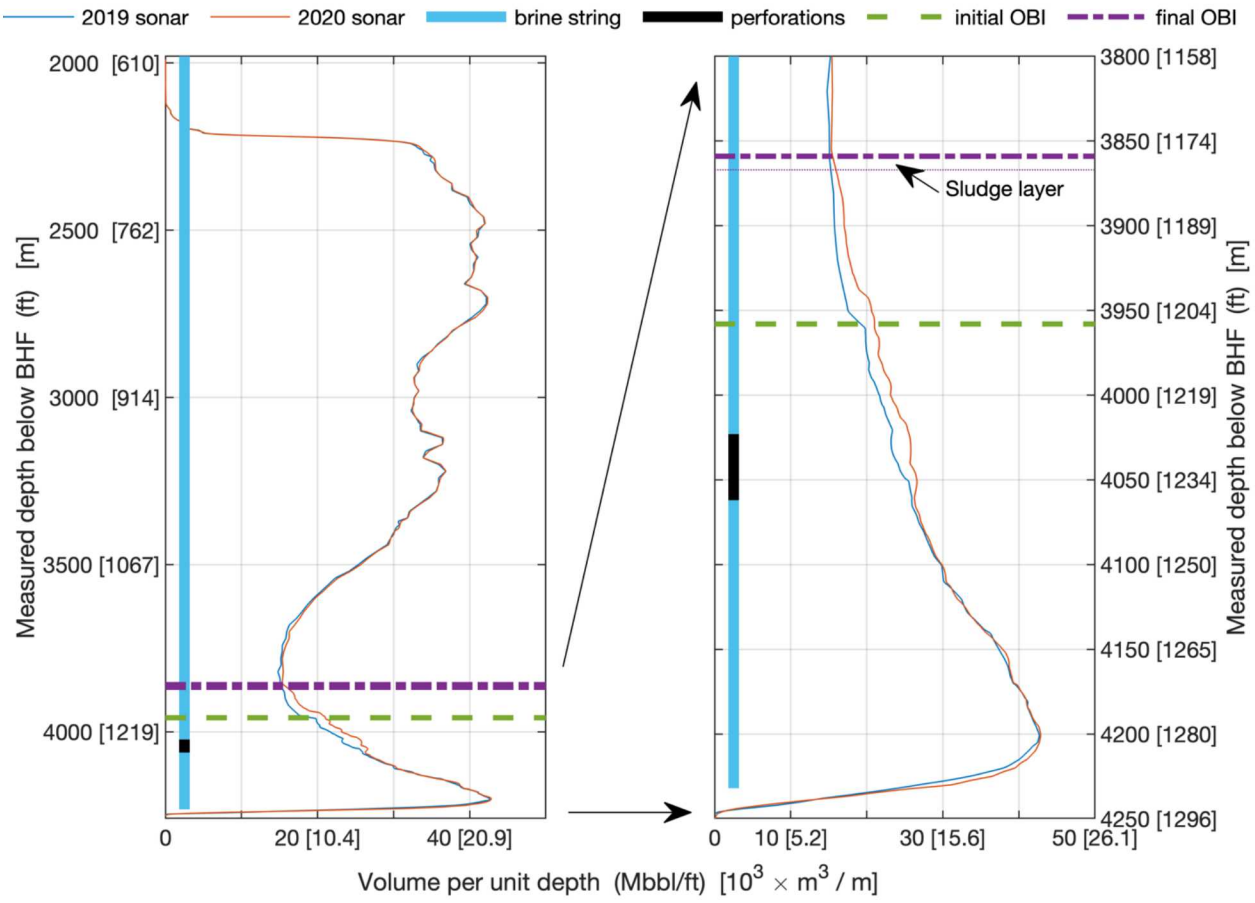

Figure 12 Volume curve for cavern BM-102. Left: full cavern depth range. Right: zoomed view of the curves from the cavern floor to just above the final OBI after sales. The brine string & perforations are shown for depth reference purposes only.

Once focused to the area below the final OBI, the leaching profile becomes obvious. The leached portion of the cavern extends from slightly below the bottom of the perforations and continues upwards to the final oil interface; in this case, a thin layer of sludge was created between the brine and oil, and the interface used is the top of the sludge layer. The remaining areas of difference fall within the sonar survey margins of error for volume. Of particular importance, there is no evidence of leaching at the bottom of the cavern which shows that there was no significant flow of raw water out the bottom of the BS.

Integrating volumes in only the section between 4070 to 3850 ft MD (1241–1173 m MD), the total volume within the area of interest can be calculated. The 2019 volume between these two depths is 765 Mbbl (122,000 m^3). The 2020 volume between these two depths is 826 Mbbl (131,000 m^3). Assuming that the 1% error metric is valid for large-enough subsections of the cavern, then the range of possible differences in volume can be calculated. These error bar calculations are shown in Table 4, and are shown graphically in Figure 13.

Table 4 Calculated ranges of change in volume between just below the bottom of the perforated section of the BS and just above the top of the final oil-sludge interface.

	2019 Sonar	2020 Sonar
Calculated volume between bottom of perfs. and final OBI	765 Mbbl *122×10³ m³*	826 Mbbl *131×10³ m³*
+1% upper error bound	773 Mbbl *123×10³ m³*	834 Mbbl *132×10³ m³*
-1% lower error bound	757 Mbbl *121×10³ m³*	817 Mbbl *130×10³ m³*
Range for change in volume	817-773 = 44 (lower bound), 834-757 = 77 (upper bound): 44 to 77 Mbbl *7,000 to 11,000 m³*	

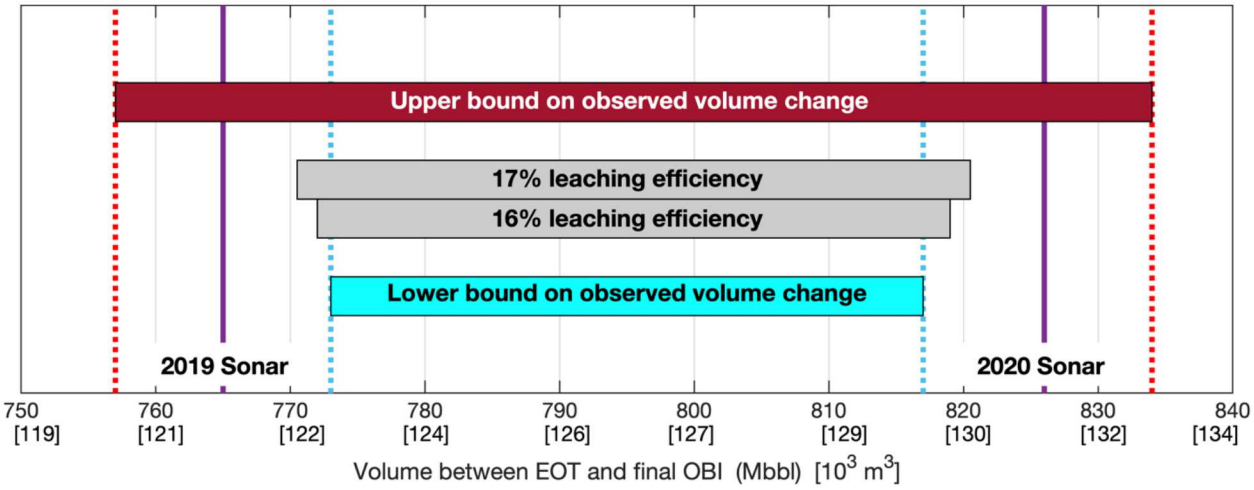

Figure 13 Observed sonar volumes with 1% error bounds. Upper bound on the observed change in volume shown in dark red; lower bound on the observed change in volume shown in cyan. The expected change in volume due to leaching is shown in the middle.

Figure 13 shows that the change in volume, in the area between the bottom of the perforations and the final OBI, is consistent with the expected change due to leaching (in gray). When the possible salt fall/missed feature discussed previously is also taken into account, it only improves the fit. Thus, it can be concluded that the mitigation technique of perforating the brine string was successful in redirecting all flow through the perforations and avoiding a sharp ledge or flipper being created.

Conclusion

Due to the unique situation at the U.S. Strategic Petroleum Reserve, raw water must be used for the release of oil. Using a split shot or jet cutter to change the brine string depth, and thus change the location where leaching occurs within the cavern due to raw water injection, has significant drawbacks. Using perforation tools to create a flow path higher in the brine string, without cutting it completely, was investigated by the SPR.

The mathematical model developed by Sandia National Laboratories provided a simplified approximation for calculating the critical velocity where flow would stop fully exiting through the perforations and start to exit through the end of tubing. Fluor Federal Petroleum Operations worked with their wireline vendor to

test perforation tools on SPR sized tubing at both the bench scale and in a simple down-hole test where the piping was recovered. A full-scale test of the perforation process was then conducted during Congressionally mandated oil sales in October and November of 2019. Sandia and FFPO worked together to evaluate the results of the test using pre- and post-sales sonar surveys of the cavern.

The initial field test demonstrated that, without a centralizer, hole diameters significantly varied due to the angle and water gap of the tool within the relatively large tubing (compared to tool size). Discovering these variations, and their range, was critical in ensuring that the correct average surface area for the perforations could be used when calculating the number of perforations required.

The mathematical model was used to build a tool that would calculate flow rates out the perforations versus flow out the EOT. The tool was used to verify that the final gun configuration would be sufficient to keep flow exclusively out the perforations at the flow rates planned for sales. The result was a configuration where 720 holes were created over 39 feet (10 meters) of tubing in the sales test cavern.

The final sale involved the injection of just under 300 Mbbl (47.7×10^3 m^3) of raw water into the cavern. Analysis of flow rates and differential pressures indicated no problems with flow through the perforations that would damage the SPR infrastructure or limit delivery targets. Comparison of the pre- and post-sales sonars shows that the leaching occurred only in the desired regions – from the perforations up to the oil interface – and the observed leaching was consistent with expected leaching efficiency; the expected volume change (47-50 Mbbl, or 7500-7900 m^3) falls within the error bounds of the observed leaching (44-77 Mbbl, or 7000-11000 m^3).

Based on these results, the field test of brine string perforations in Cavern BM-102 was successful. Using perforations to avoid undesirable preferential leaching at the foot of a cavern is a viable alternative to cutting a hanging string, and the leaching was well distributed across the perforations and up to the oil-sludge-brine interface.

Acknowledgements

Special thanks to: Lauren Ramsey, Jerry Smart and Greg Carson, at FFPO, who were instrumental in data collection of the perforation test on WH-109 and execution of perforating on BM-102B; to Kirsten Chojnicki and Todd Zeitler at SNL for their work on leaching and string cuts which informed the selection of BM-102 for this study; to Barry Roberts at SNL for sonar survey analysis advice; to Raquel Valdez, student intern at Sandia from the University of New Mexico, for assistance with the graphics; and to the many people at the DOE SPR Project Management Office in New Orleans, LA.

References

(BAILEY 1975) B. J. Bailey, “Fluid Flow in Perforated Pipes,” *Journal of Mechanical Engineering Science*, **17** (6), 338-347, 1975.

(BATCHELOR 1967) G. K. Batchelor, *An Introduction to Fluid Dynamics*, Cambridge University Press, Cambridge, UK, 1967, Section 6.3.

(CLEMO 2006) T. Clemo, “Flow in perforated pipes: a comparison of models and experiments.” *SPE Production & Operations*, **21** (2), 302-311, 2006.

(NEMER AND KASSAM 2019) M. B. Nemer and I. A. Kassam, “Flow through Perforated Pipe,” internal memorandum, Sandia National Laboratories, Albuquerque, NM, May 31, 2019.

(RUSSO 1983) A. J. Russo, *A User’s Manual for the Salt Solution Mining Code, SANSMIC*, report SAND83-1150, Sandia National Laboratories, Albuquerque, NM, 1983.

(TORCZYNSKI 2019) J. R. Torczynski, “Strategic Petroleum Reserve (SPR): Model for Buoyant Flow in a Perforated Hanging String,” internal memorandum, Sandia National Laboratories, Albuquerque, NM, August 13, 2019.

(WEBER ET AL. 2016) P. D. Weber, B. L. Roberts, and D. K. Rudeen, *SANSMIC User Manual*, report SAND2016-8350, Sandia National Laboratories, Albuquerque, NM, 2016.

(WOLFRAM 2019) Wolfram, *Mathematica*, https://www.wolfram.com/mathematica/, 2019.